NANO LETTERS

2007
Vol. 7, No. 5
1369−1375

Designing Catalytic Nanomotors by Dynamic Shadowing Growth

Yuping He, Jinsong Wu, and Yiping Zhao*

Department of Physics and Astronomy, and Nanoscale Science and Engineering Center, University of Georgia, Athens, Georgia 30602

Received February 26, 2007; Revised Manuscript Received April 1, 2007

ABSTRACT

Using a geometric shadowing effect, a thin catalyst layer can be coated asymmetrically on the side of a nanorod backbone. Combining with substrate rotation, a dynamic shadowing growth technique has been developed to fabricate catalytic nanomotors such as rotary Si/Pt nanorods, rotary L-shaped Si/Pt and Si/Ag nanorods, and rolling Si/Ag nanosprings, and their autonomous motions have been demonstrated in a diluted H_2O_2 solution. This fabrication method reveals an optimistic step toward designing integrated nanomachines.

Introduction. Controlled motion of nanoscale objects is the first step to achieve integrated nanomachinary systems that can enable breakthrough applications in nanoelectronics, photonics, bioengineering, drug delivery, and disease treatment. Naturally occurring nanomotors are biological motor proteins powered by catalytic reactions.[1−4] Unlike the nanomotors in nature, most artificial nanomotors are usually powered by external fields.[5−15] One significant advantage of the bionanomotor is the use of chemicals, through a catalytic reaction, to fuel its motion. To mimic this mechanism, a catalytic reaction can be introduced to an inorganic nanosystem to achieve desirable motions. These catalytic nanomotors, independently demonstrated by Mallouk and Sen's groups at Pennsylvania State University[16] and Ozin's group at University of Toronto,[17] have captured the essential idea of "fueling" the nanomachine and translating the catalytic reaction energy to kinetic energy for nanorod motion. The nanomotors produced in these two groups are coaxial Au−Pt[16] and Au−Ni[17] heteronanorod structures fabricated through template-directed electroplating (TDEP), and the fuel to power the motion is H_2O_2 solution. Both Pt and Ni can act as a catalyst to decompose H_2O_2 locally into H_2O and O_2, which turns the chemical energy into mechanical energy. A key design rule for those catalytic nanomotors is the asymmetric deposition of a catalytic section/layer onto the nanorod structure, an idea inspired by the work done in Whitesides' group.[18] However, although they have fabricated similar structured nanorods, the Penn State group and the Toronto group observed two different motion behaviors. The Penn State group found that the Au−Pt nanorods were performing a translational motion in H_2O_2 solution, and the motion direction is from Au to Pt, i.e., there is a force pulling the nanorod toward to Pt section. Their recent experiments demonstrated that the pulling mechanism is due to an electrochemical pathway between Au and Pt during the H_2O_2 decomposition.[19] Very recently, they have also successfully observed similar motion behaviors in other coaxial heteronanorod systems such as Ru−Au, Pd−Au, Au−Ru, etc.[20] The motion observed by the Toronto group is a rotary motion with one end of the nanorod anchored on a substrate.[17] They believe the driving force is due to the nanobubbles of O_2 evolved from the H_2O_2 catalytic decomposition.[21] This discrepancy in motion mechanism will affect the nanomotor design and deserves more detailed study. With the success in catalytic nanomotors, the Penn State group also demonstrated the ideas of micropumps,[22] microgears,[23] and controlled motion of nanomotors using magnetic layer.[24] Other groups have demonstrated glucose-fueled bioelectrochemical motors[25] and catalytic molecular motors.[26] Within the past few years, the concept of catalytic nanomotors has been demonstrated as one of the most promising mechanisms for future nanomachine applications.

However, to mimic many complicated motions that occur in bionanomotors in a controlled fashion, such as rotation, rolling, shuttling, delivery, contraction, etc., it requires one to design the nanomotors to be able to perform different motions or to design components that have the capability to achieve those motions once they are integrated together. Thus, the first challenge for designing a catalytic nanomotor is whether one can fabricate different catalytic motors with different motion behaviors. The fabrication technique should also be flexible enough for future integration and functionalization. An ideal nanofabrication method for catalytic nanomotor production should have the ability to coat the catalytic layer asymmetrically onto nanorod backbones and at the same time be able to control this coating in a manner that produces different motions. Therefore, a fabrication

* Corresponding author. E-mail: zhaoy@physast.uga.edu.

10.1021/nl070461j CCC: $37.00
Published on Web 04/13/2007

technique that can control the backbone deposition and asymmetric catalyst coating simultaneously is needed. For the catalytic nanomotors demonstrated so far, they are mainly fabricated by the TDEP method.[16,17] TDEP is a template method,[27] and it is a simple, low-cost method that can fabricate various materials at low temperature. However, the size of the nanorod is limited by the size of the nanochannel in the template. The deposited material is limited by the electrolyte solution, and the substrate has to be conductive. Therefore, for catalytic nanomotor fabrication, the TDEP method may have the following disadvantages: (1) It can only produce coaxial nanostructures. Therefore, only limited motion style may be produced. (2) Although there are successes in controlling the motion behaviors by an external magnetic field, the motion cannot be controlled by a chemical environment, i.e., "on-board" fuel. (3) Materials are limited for the current plating technique, which limits the ability for future integration and functionalization. (4) The fabrication technique is not compatible with the microfabrication process. That may affect future large-scale integration and production.

Here, we demonstrate a simple but versatile technique to fabricate catalytic nanomotors by dynamic shadowing growth (DSG), which is based on shadowing effect and dynamic substrate manipulation in a physical vapor deposition system. The geometric shadowing effect during thin film deposition is essentially an asymmetric coating method. DSG can provide more flexibility for designing desired nanomotor structures when combining with substrate rotation. With the asymmetric deposition from DSG, we design Si/Pt or Si/Ag nanomotors with different shapes and demonstrate their catalytic motion behaviors.

Designing a Rotary Si/Pt Nanorod Nanomotor. The basic principle for catalytic nanomotor fabrication is to break the symmetry during catalyst deposition. To achieve such a deposition, we employ a dynamic shadowing growth (DSG) process. The essence of DSG process is illustrated in Figure 1 to fabricate the Si/Pt nanorod nanomotors. This is a two-step fabrication process: the first step is to deposit the Si nanorod backbones, and the second step is to deposit the Pt, the catalyst layer, asymmetrically on one side of the Si nanorod backbones. A layer of Si backbone nanorod array is first fabricated by oblique angle deposition (OAD). OAD is a physical vapor deposition technique in which the incident Si vapor atoms are deposited on a substrate at a large incident angle θ (>70°) with respect to the surface normal of the substrate. Because of the shadowing effect and surface diffusion, aligned nanorods are formed, tilting away from the substrate normal at an angle of β. In general, $\beta < \theta$. After Si nanorod deposition, a very thin layer of Pt is deposited perpendicular to the substrate (Figure 1b). Because the Si nanorods already have an angle with respect to the substrate normal, the shadowing effect causes the Pt layer to deposit only onto one side of the Si nanorod, as long as the thickness of the Pt layer is thinner than the gap a between two adjacent Si nanorods. The gap a is determined by the average separation Δd between two adjacent Si nanorods and β (Figure 1b), $a = \Delta d \cos \beta$. According to the geometric

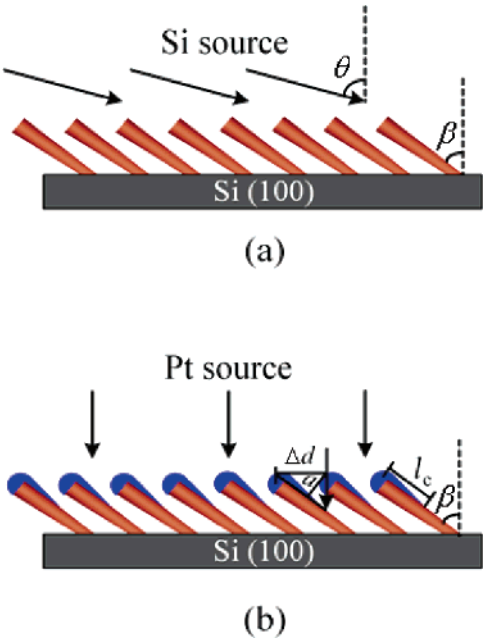

Figure 1. Fabrication procedure of Si/Pt nanorod nanomotors.

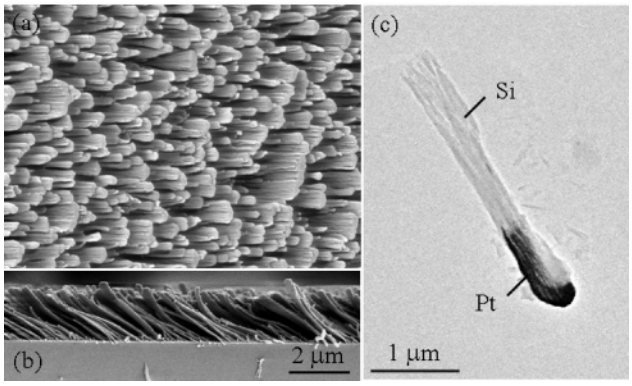

Figure 2. SEM top view (a), cross-sectional view (b), and TEM (c) images of Si/Pt nanorods.

shadowing effect, the length l_c of the coated Pt layer can be estimated as $l_c = \Delta d/\sin \beta$. In the experiment, the Si nanorods were fabricated in a high vacuum chamber with a background pressure of 4×10^{-6} Torr. The Si (99.9995%, from Alfa Aeser) source was evaporated by electron beam bombardment. The pressure during deposition was less than 1×10^{-5} Torr, and the growth rate was monitored by a quartz crystal microbalance (QCM). The vapor incident angle θ was fixed at 86°. The distance between the evaporation source and the substrate was approximately 30 cm. During the deposition, the deposition rate was controlled at 0.5 nm/s. These fabrication conditions were used to fabricate all the Si nanorods in this letter. A layer of Si nanorods with 4 μm nominal thickness (QCM reading) were deposited on Si (100) substrate. After the Si nanorod deposition, an asymmetrical layer of Pt film was coated on one side of the Si nanorods by thermal evaporation, and the Pt vapor flux was incident to the sample surface along the substrate normal.

The structures and morphologies of the fabricated nanomotors were observed by a transmission electron microscopy (TEM, FEI Tecnai 20) and a field emission scanning electron

Figure 3. Snapshots of a typical rotary motion of a Si/Pt nanorod. The time interval between two adjacent frames is 0.1 s. In the experiment, both the clockwise and counterclockwise rotations have been observed due to the random orientations of the nanorods in the solution.

microscope (SEM, LEO 982). Figure 2 shows the SEM and TEM images of the Si/Pt nanorods. Because the Si deposition was carried out at room temperature, the resulting Si nanorods were amorphous, i.e., the Si rods can be treated as insulating rods. The Si nanorods are not cylindrical, but rather, their cross sections are prolate. The average size is estimated to be 3.0 μm long, 0.35 μm wide, and 0.1 μm thick. The density of the nanorods is approximately $2.0 \times 10^9/\text{in}^2$, and the tilting angle $\beta \approx 55°$. Thus $\Delta d \approx 0.92$ μm, $a \approx 0.53$ μm, and $l_c \approx 1.12$ μm. Figure 2c shows a typical TEM image of the Si/Pt nanorods. The light section is the Si nanorod and the dark section is the Pt coating. The image contrast results from the different scattering cross sections of electrons in Si and Pt due to different atomic masses. According to multiple TEM images obtained in the experiment, the Pt coating is approximately 0.14 μm thick and 1−2 μm long on one side of the Si nanorods. The coating results are consistent with the calculated values.

The motions of nanomotors were recorded with and without H_2O_2 solution using an optical microscope (Mitutoyo FS-110) equipped with a CCD camera. The nanomotors were ultrasonically separated from the Si substrate and dispersed in water solution. A drop (~10 μL) of Si/Pt nanorod suspension was injected onto a clean silicon wafer and then the 5.0% (in mass) H_2O_2 solution of 10−40 μL was added. In the absence of H_2O_2, i.e., in DI water, the Si/Pt nanorods only perform a random Brownian motion. Once the H_2O_2 solution is added, most of the Si/Pt nanorods start to rotate around a fixed point at/near one end of nanorod, and both the clockwise and counterclockwise rotations have been observed due to the random orientations of the nanorods in the solution. Other motions such as precession, flipping, and translational motion, were obtained occasionally. All of these behaviors are related to the nature of the Pt coating on an individual nanorod backbone. Figure 3 shows a typical rotary evolution of a single Si/Pt nanorod (see video in Supporting Information showing both the clockwise and counterclockwise rotations). The arrow in each frame denotes the orientation of the nanorod. The rotation period is measured to be $T = 1$ s. Clearly, the rotation is due to the asymmetrical deposition of the Pt catalyst layer on the side of the Si nanorod. Comparing this with the Au−Pt or Au−Ni coaxial structures reported in the literature,[16,17] the side coating of the catalyst layer is ready to generate a torque to rotate the nanorod. However, due to the symmetry of the nanorod, one cannot tell the direction of the propelling force, i.e., whether it is pushing or pulling the nanorod from the Pt surface.

Designing L-Shaped Si/Pt and Si/Ag Nanorod Nanomotors. To determine the direction of the propelling force, we design an L-shaped nanomotor of two arms with different

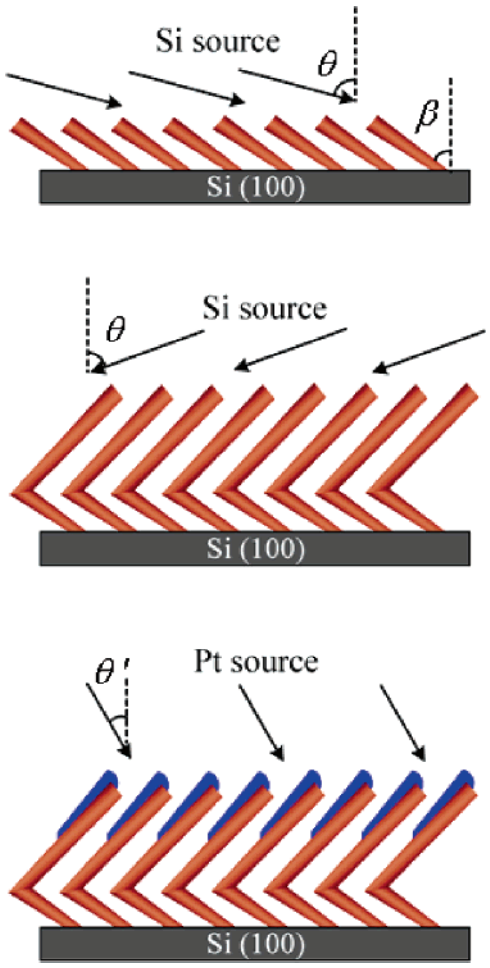

Figure 4. Fabrication procedure of L-shaped Si/Pt nanorod nanomotors.

lengths. The fabrication process for the L-shaped Si/Pt nanorod nanomotors is illustrated in Figure 4. First, a layer of tilted short Si nanorods of 4 μm nominal thickness were grown by oblique angle deposition, using the same growth conditions as described in the previous section. Then the substrate was rotated 180° azimuthally at a very fast rotation rate. Another layer of long Si nanorods of 6 μm nominal thickness were deposited so that one could distinguish these two arms by length under optical microscope. Finally, a layer of Pt thin film was thermally evaporated on the outer arm of the L-shaped Si nanorod with the substrate tilted at a small angle θ' of 5−10°. We hoped that this small tilting angle would help to improve the uniformity of the Pt coating on the Si nanorods because, at normal deposition angle, as shown in Figure 2c (TEM image of Si/Pt nanorods), the top of the Si nanorod is covered heavily with a layer of Pt film. Figure 5 shows the SEM and TEM images of the L-shaped

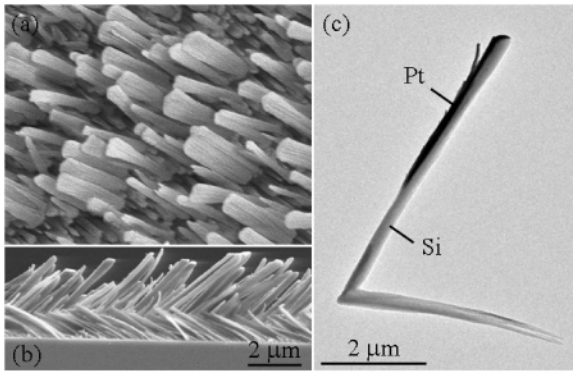

Figure 5. SEM top view (a), cross-sectional view (b), and TEM (c) images of L-shaped Si/Pt nanorods.

Si/Pt nanorods. The nanorod consists of two arms, a long arm approximately 3.6 μm long, 0.7 μm wide, and 0.16 μm thick, with Pt coating, and a short arm approximately 2.6 μm long and 0.16 μm thick. These two arms form an angle of 70°. The Pt coating is approximately 0.08 μm thick and 1.5−3.6 μm long on the side of the long arm (Figure 5c). Compared with Figure 2c, the uniformity of the Pt coating is improved on the nanorods.

The motions of the L-shaped Si/Pt nanorods were observed in 5% H_2O_2 solution. A typical rotary motion of an L-shaped Si/Pt nanorod is shown in Figure 6 (see video in Supporting Information). The rotation period is $T = 4$ s. This nanomotor rotated closely around a fixed point near the joint of both arms. Although we also observed both the clockwise and counterclockwise rotations for the L-shaped nanorods due to their random orientations, we found that all the rotary L-shaped nanorods rotated from the long arms to the short arms regardless of their apparent rotation directions (clockwise and counterclockwise). From the design of the L-shaped nanorod, we can conclude that the nanorods are pushed from the Pt side. The observed motion of the L-shaped Si/Pt nanomotor clearly demonstrated the direction of the propelling force for the Si/Pt catalytic nanomotor: the catalytic reaction on the surface of the Pt layer generates a propelling force to push the nanorod from the Pt side. Currently, the exact origin of this force is not clear. One possible reason is due to the burst of small O_2 bubbles on the Pt surfaces, similar to the observations by Whitesides[18] and Ozin.[17] This observation is very different from those reported by the Penn State group, where the force is pulling toward the Pt end in the Au−Pt structure due to electrochemically induced interaction.[19,20,28] Our material system, the Si/Pt nanorods, an insulator/metal structure, is different from their coaxial bimetallic structures. Therefore, there is no electrochemical pathway able to induce electrokinetics in our Si/Pt nanorods when immersed in H_2O_2 solution.

Considering the viscous drag of the solution, the force analysis for a free Si/Pt nanorod nanomotor is illustrated in Figure 7. There are two main forces exerted on both nanorods, the propelling force F_{drive} caused by the H_2O_2 catalytic reaction, and the viscous drag force resulting from the motion in a fluid. Other forces, such as supporting force or friction, when one end of the nanorod is anchored to a surface, have been neglected. We also neglected a small driving force that could occur on the tip of the Si nanorod due to the capped Pt layer. For a rod rotating around one end, the viscous dragging force can be estimated by the following equation:[29]

$$F_{drag} = \frac{4\pi\mu l}{\ln(2l/r) + 0.5} v$$

where l and r are the length and radius of an uniform straight rod, μ is the viscosity of the liquid (0.001 Ns/m^2 for water), and v is the linear speed at the other end of rod. In our case, the nanorods are not very uniform, so their centers of mass may deviate from their midpoints and will be different from one another. The center of mass of nanorod is determined by its shape and uniformity, which are related to the parameters r and l. Here, we use the average r and l values obtained from the SEM images to estimate the force. In addition, the dragging force in the L-shaped nanorod is estimated by simply adding the two dragging forces from the two sections of the L-shaped nanorod. The estimated force for the Si/Pt nanorod nanomotor is $F_{drive} = -F_{drag} \approx 1.8 \times 10^{-13}$ N, and for the L-shaped Si/Pt nanorod nanomotor, $F_{drive} = -F_{drag} \approx 5.8 \times 10^{-14}$ N. Those values are consistent with the reported values for other catalytic nanomotors.[16]

We have also used Ag as the catalyst instead of Pt and designed a four-layer L-shaped Si/Ag nanorod nanomotor of two Si arms with different lengths. It consists of two nanorod nanomotor (in Figure 1) components, as sketched in Figure 8a. After growing the first layer of tilted short Si nanorods of 4 μm nominal thickness at $\theta = 86°$, without breaking the vacuum, a thin layer of Ag of 0.1 μm nominal thickness was deposited in the same chamber at a small deposition angle θ' of 5−10° (shown in Figure 4). The deposition rate of Ag source was fixed at 0.2 nm/s. Then the substrate was rotated 180° azimuthally, and using the same conditions, another layer of long Si nanorods of 7 μm nominal thickness and an Ag film of 0.1 μm nominal thickness were deposited subsequently. The typical TEM image is shown in Figure 8b. Combining with SEM images (not shown), the long Si arm is approximately 4.4 μm long, 1.1 μm wide, and 0.3 μm thick, with the side coated by Ag approximately 0.1 μm thick and 2.0−4.4 μm long. The short

Figure 6. Snapshots of a typical rotary motion of an L-shaped Si/Pt nanorod. The time interval between two adjacent frames is 0.4 s. For this case, we also observed both the clockwise and counterclockwise rotations.

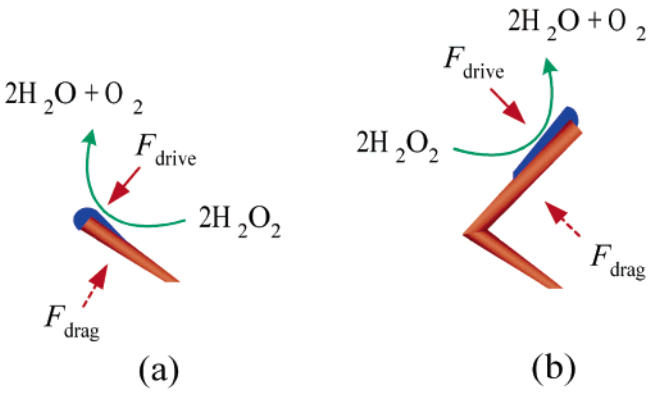

Figure 7. Force analysis for rod-shaped and L-shaped Si/Pt nanorods.

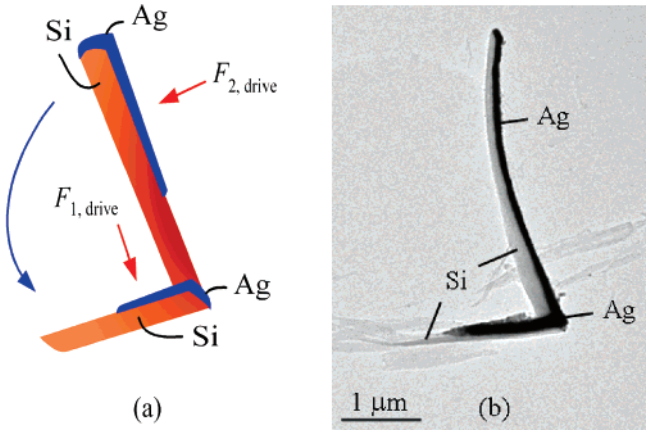

Figure 8. (a) Sketch of L-shaped Si/Ag nanorod and force analysis. (b) TEM image of an L-shaped Si/Ag nanorod.

Si arm is approximately 2.6 μm long and 0.2 μm thick, coated by Ag approximately 0.1 μm thick and 1.0−1.5 μm long. The included angle of the two arms is approximately 70°.

For Ag catalyst, we found 5.0% H_2O_2 could produce a lot of visible bubbles, unfavorable for motion observation. To avoid this, the H_2O_2 fuel was further diluted and a concentration of 1.5% was used. We believe that, by using Ag instead of Pt, the role of the catalytic reaction in the motion keeps invariant: the L-shaped Si/Ag nanorods are pushed from the Ag sides and thus rotate from the long arms to short arms (see video in Supporting Information, showing both the clockwise and counterclockwise rotations), as expected in Figure 8a. On the average, the rotary period $T \approx 1.3$ s, and thus the total driving force $F_{drive} = -F_{drag} \approx 3.1 \times 10^{-13}$ N. Compared with Pt, qualitatively, Ag is more active than Pt in H_2O_2 catalytic reaction, but Ag is prone to be poisoned due to surface oxidation in view of the loss of its catalytic activity during H_2O_2 decomposition. A detailed comparison on the catalytic properties of Ag and Pt is under investigation.

Designing a Rolling Nanomotor: The Si/Ag Nanospring. Once we understood that the catalytic reaction generated a propelling force to push the catalyst layer, we could design a complex nanomotor structure capable of performing complicated motion. One such complex structure is a rolling nanospring, as illustrated in Figure 9. First, a

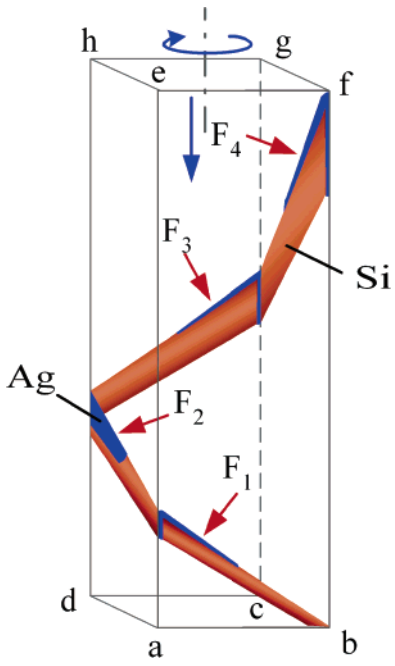

Figure 9. Sketch of Si/Ag nanospring structure and force analysis.

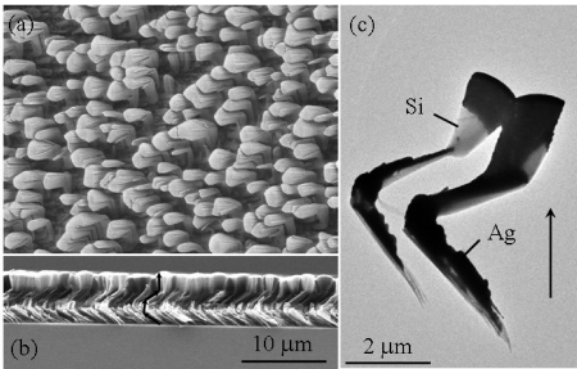

Figure 10. SEM top view (a), cross-sectional view (b), and TEM (c) images of Si/Ag nanosprings. The arrows in (b) indicate the growth sequence in a nanospring. The arrow in (c) denotes the growth direction.

layer of tilted Si nanorods was deposited in the a−e−f−b plane at a large oblique angle ($\theta = 86°$). Without breaking the vacuum, a thin layer of Ag was deposited on the same plane with a small deposition angle θ' of 5−10°. Then the substrate was fast rotated 90° counterclockwise. Then another layer of tilted Si nanrods was deposited on the d−h−e−a plane at a large oblique angle ($\theta = 86°$), followed by a thin Ag layer deposition at θ' of 5−10°. Repeating this process two more times, one can obtain a structure similar to Figure 9. The nominal thicknesses of Si nanorods and Ag film in each layer are 4 and 0.1 μm, respectively. If this structure is placed into H_2O_2 solution, according to our understanding of the propelling force, we expect a propelling force F_1 exerted perpendicular to the arm of the nanospring on the a−e−f−b plane. Similar propelling forces, F_2, F_3, and F_4, exist perpendicular to the arms on the planes of d−h−e−a, c−g−h−d, and b−f−g−c, respectively. The net results of these four forces are a net torque and a net force pointing downward along the axis of the spring. Thus, we expect that

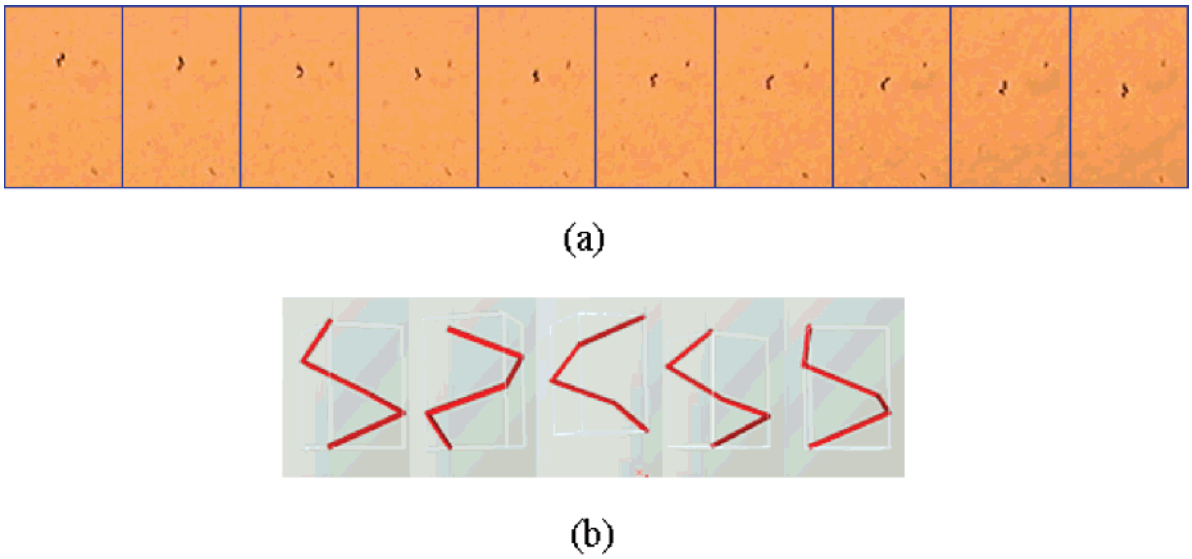

Figure 11. (a) Snapshots of a typical rolling motion of a Si/Ag nanospring. The time interval between two adjacent frames is 0.2 s, and the rotation direction is clockwise. (b) A square nanospring rotates clockwise at different phases simulated by AutoCAD.

the Si/Ag nanospring will rotate clockwise about its axis while moving downward once placed into H_2O_2 solution. In fact, we have fabricated such Si/Ag nanosprings according to the above procedure using the multilayer DSG technique. The SEM and TEM images shown in Figure 10 clearly demonstrate the spiral structure of the Si/Ag nanosprings, and the arrows in Figure 10b illustrate the growth directions. From the substrate to the top of the nanospring, the arrows change direction four times, which represents four arms and one complete turn of the nanospring. We also observe that the arms grow thicker and thicker with increasing layers (Figure 10c). The Ag layer was coated on the sides of all the arms. The average length of the Si nanorod arms is approximately 2.5 μm, the average diameter of the nanorods in the top layer is approximately 1.6 μm, and the Ag coating is approximately 0.2 μm thick and 1.0−2.5 long.

When the Si/Ag nanosprings were placed in 1.5% H_2O_2 solution, we indeed observed the rolling and translational motions of the nanosprings. The snapshots of the motion are illustrated in Figure 11a (see video in Supporting Information). The rolling direction is clockwise, accompanied by a downward translational motion. This motion is consistent with the expected motion described in Figure 10. Because the nanostructure is in three dimensions, while the movie taken only reflects the plane projection of the structure, it is hard to tell the rotation direction without dispute. One can use three-dimensional graphic software, AutoCAD, to simulate the plane clips, as illustrated in Figure 11b, which provides a powerful tool to help one to understand the complicated motion behaviors of the complex nanomotors. The rolling period is estimated to be $T = 1.8$ s. Within one period, the nanomotor translates along the central axis for a distance of ~11.4 μm. Thus the translational speed is approximately 6.3 μm/s.

Conclusions. A DSG technique, based on shadowing effect and substrate rotation, has been developed capable of successfully fabricating catalytic nanomotors with different geometries and controlled motions, such as rotary Si/Pt nanorods, rotary L-shaped Si/Pt and Si/Ag nanorods, and rolling Si/Ag nanosprings. According to the SEM and TEM characterization, the catalyst Pt or Ag layer is coated onto the Si nanorod backbone asymmetrically. Their observed catalytic motion behavior in 1.5−5.0% H_2O_2 solution demonstrates that the H_2O_2 catalytic decomposition on the surface of the catalyst generates a propelling force that pushes the nanorod from the catalyst side with an estimated driving force on the order of 10^{-13}−10^{-14} N. These results reveal that: (1) the DSG technique has a unique asymmetric growth nature with relation to the design of the catalyst layer; (2) by combining with multilayer deposition, one can design complex nanostructures to achieve different motions; (3) it is possible to use the controlled nanomotors to assemble complicated nanomachines or use them as vehicles for drug delivery or other applications. In addition, the achievement of controlled motions is important to the understanding of catalytic motion mechanisms. With these advantages, we believe we are ready to produce complex catalytic nanomotors with complicated motion behaviors.

Acknowledgment. This work was partly supported by a DOE Hydrogen Initiative Award (DE-FG02-05ER46251) and a NSF NER Award (ECS-0404066). We thank Yongjun Liu for helping with the AutoCAD drawing and Chris Hoffmann for proofreading the manuscript.

Supporting Information Available: A video of rotary Si/Pt nanorods in 5.0% H_2O_2 solution; a video of an L-shaped Si/Pt nanorod in 5.0% H_2O_2 solution and a video of L-shaped Si/Ag nanorods in 1.5% H_2O_2 solution, both demonstrating that the nanorods are rotating from long arms to short arms; a video of a rolling Si/Ag nanospring in 1.5% H_2O_2 solution (all .avi). This material is available free of charge via the Internet at http://pubs.acs.org.

References

(1) Banta, S.; Megeed, Z.; Casali, M.; Rege, K.; Yarmush, M. L. *J. Nanosci. Nanotechnol.* **2007**, *7*, 387−401.

(2) Hess, H. *Soft Matter* **2006**, *2*, 669−677.
(3) Schliwa, M.; Woehlke, G. *Nature* **2003**, *422*, 759−765.
(4) Soong, R. K.; Bachand, G. D.; Neves, H. P.; Olkhovets, A. G.; Craighead, H. G.; Montemagno, C. D. *Science* **2000**, *290*, 1555−1558.
(5) Fennimore, A. M.; Yuzvinsky, T. D.; Han, W. Q.; Fuhrer, M. S.; Cumings, J.; Zettl, A. *Nature* **2003**, *424*, 408−410.
(6) Fan, D. L.; Zhu, F. Q.; Cammarata, R. C.; Chien, C. L. *Appl. Phys. Lett.* **2004**, *85*, 4175−4177.
(7) Fan, D. L.; Zhu, F. Q.; Cammarata, R. C.; Chien, C. L. *Phys. Rev. Lett.* **2005**, *94*, 247208.
(8) Regan, B. C.; Aloni, S.; Jensen, K.; Ritchie, R. O.; Zettl, A. *Nano Lett.* **2005**, *5*, 1730−1733.
(9) Edwards, B.; Mayer, T. S.; Bhiladvala, R. B. *Nano Lett.* **2006**, *6*, 626−632.
(10) Vickrey, T. M.; Garciaramirez, J. A. *Sep. Sci. Technol.* **1980**, *15*, 1297−1304.
(11) Watarai, H.; Suwa, M.; Iiguni, Y. *Anal. Bioanal. Chem.* **2004**, *378*, 1693−1699.
(12) Bentley, A. K.; Trethewey, J. S.; Ellis, A. B.; Crone, W. C. *Nano Lett.* **2004**, *4*, 487−490.
(13) Grier, D. G. *Nature* **2003**, *424*, 810−816.
(14) Galajda, P.; Ormos, P. *Appl. Phys. Lett.* **2002**, *80*, 4653−4655.
(15) Huang, W.; Qian, W.; El-Sayed, M. A. *J. Am. Chem. Soc.* **2006**, *128*, 13330−13331.
(16) Paxton, W. F.; Kistler, K. C.; Olmeda, C. C.; Sen, A.; St Angelo, S. K.; Cao, Y. Y.; Mallouk, T. E.; Lammert, P. E.; Crespi, V. H. *J. Am. Chem. Soc.* **2004**, *126*, 13424−13431.
(17) Fournier-Bidoz, S.; Arsenault, A. C.; Manners, I.; Ozin, G. A. *Chem. Commun.* **2005**, 441−443.
(18) Ismagilov, R. F.; Schwartz, A.; Bowden, N.; Whitesides, G. M. *Angew. Chem., Int. Ed.* **2002**, *41*, 652−654.
(19) Paxton, W. F.; Baker, P. T.; Kline, T. R.; Wang, Y.; Mallouk, T. E.; Sen, A. **2006**, *128*, 14881−14888.
(20) Wang, Y.; Hernandez, R. M.; Bartlett, D. J., Jr.; Bingham, J. M.; Kline, T. R.; Sen, A.; Mallouk, T. E. *Langmuir* **2006**, *22*, 10451−10456.
(21) Ozin, G. A.; Manners, I.; Fournier-Bidoz, S.; Arsenault, A. *Adv. Mater.* **2005**, *17*, 3011−3018.
(22) Kline, T. R.; Paxton, W. F.; Wang, Y.; Velegol, D.; Mallouk, T. E.; Sen, A. *J. Am. Chem. Soc.* **2005**, *127*, 17150−17151.
(23) Catchmark, J. M.; Subramanian, S.; Sen, A. *Small* **2005**, *1*, 202−206.
(24) Kline, T. R.; Paxton, W. F.; Mallouk, T. E.; Sen, A. *Angew. Chem., Int. Ed.***2005**, *44*, 744−746.
(25) Mano, N.; Heller, A. *J. Am. Chem. Soc.* **2005**, *127*, 11574−11575.
(26) Vicario, J.; Eelkema, R.; Browne, W. R.; Meetsma, A.; La Crois, R. M.; Feringa, B. L. *Chem. Commun.* **2005**, 3936−3938.
(27) Kline, T. R.; Tian, M. L.; Wang, J. G.; Sen, A.; Chan, M. W. H.; Mallouk, T. E. *Inorg. Chem.* **2006**, *45*, 7555−7565.
(28) Paxton, W. E.; Sen, A.; Mallouk, T. E. *Chem.—Eur. J.* **2005**, *11*, 6462−6470.
(29) Happel, J.; Brenner, H. *Low Reynolds Number Hydrodynamics*; Noordhoff International Publishing: Leyden, The Netherlands, 1965.

NL070461J